applied optics

Substrate-free miniaturized thin-film filters for single-element coarse wavelength division multiplexing fibers

Anna K. Rüsseler,[1,2,*] Philipp Gehrke,[1] Florian Carstens,[1] Gerd-A. Hoffmann,[1,2] Guido Schönsee,[3] Axel Thiel,[3] Martina Vitt,[3] Andreas Wienke,[1,2] and Detlev Ristau[1,2,4]

[1]Laser Zentrum Hannover e.V., Hollerithallee 8, D-30419 Hannover, Germany
[2]Cluster of Excellence PhoenixD (Photonics, Optics and Engineering - Innovation Across Disciplines), Welfengarten 1a, D-30167 Hannover, Germany
[3]FOC-Fibre Optical Components GmbH, Barbara-McClintock-Str. 5, D-12489 Berlin, Germany
[4]Gottfried Wilhelm Leibniz Universität Hannover, Welfengarten 1, D-30167 Hannover, Germany
*Corresponding author: a.ruesseler@lzh.de

Received 12 October 2022; revised 22 December 2022; accepted 12 January 2023; posted 13 January 2023; published 7 February 2023

We have created high-precision, miniaturized, substrate-free filters, based on ion beam sputtering on a sacrificial substrate. The sacrificial layer is cost efficient and environmentally friendly and can be dissolved using only water. We demonstrate an improved performance compared to filters on thin polymer layers from the same coating run. With these filters, a single-element coarse wavelength division multiplexing transmitting device for telecommunication applications can be realized by inserting the filter between fiber ends. © 2023 Optica Publishing Group under the terms of the Optica Open Access Publishing Agreement

https://doi.org/10.1364/AO.478083

1. INTRODUCTION

Miniaturization of optical components lies in the focus of recent research activities, because it is a prerequisite for the development of complex but compact and cost-efficient optical systems for a wide range of applications, especially in data- and telecommunications [1]. Fiber-based wavelength division multiplexing (WDM) devices are an essential asset in this field and are commonly realized by dielectric thin-film filters. Sputter deposited thin-film coatings, e.g., produced by means of ion beam sputtering (IBS), in combination with high accuracy layer thickness monitoring form the basis for the highest spectral performance [2].

Researchers noted the great potential of thin-film filter-based WDM devices early on and proposed devices including filter coatings on glass substrates between lenses [3,4]. An accurate assembly of the lenses is necessary, and as additional elements, they contribute to the overall system cost. However, collimating lenses are required when a filter on a glass substrate with typical thicknesses of 100 µm up to several millimeters is used because otherwise the coupling efficiency to the subsequent fiber would be critically reduced. While passing such a thin-film filter, the optical radiation is no longer guided and diverges as soon as it leaves the emitting fiber. Additionally, when the beam is incident on the thin-film filter at an angle greater than 0°, the beam displacement after passing the filter element increases with the path length and thus with the substrate thickness, which is problematic for application designs with fibers. In addition to these disadvantages, the back side of the substrate has to be anti-reflection coated for minimal insertion loss (IL) in the passband [5], adding to the complexity and costs of the device.

Multiple groups have demonstrated thin-film filter-based WDM setups that do not require lenses by addressing the problem of the substrate. This includes direct coating of single-mode fiber end facets, with reported ILs of about −0.5 dB at a wavelength of 1.3 µm [6] and at shorter wavelengths [7]. Another strategy involved polishing off the excess thickness of the glass substrate and inserting the filter into a slit in the single-mode fiber. ILs of −1.44 dB to −1.7 dB at a wavelength of 1.3 µm were reported [8,9]. A more cost-efficient approach was established, based on using few-micrometer-thick spin coated layers of polyimide on silicon wafers as a substrate [10]. The thin-film filters were segmented into individual small elements, resulting in a higher yield for the filter production process, and the elements were detached at the wafer–polyimide interface. With such miniaturized filters on thin polymer substrates, various groups constructed single-mode WDM devices. Exemplary reported ILs are summarized in Table 1.

Further evolution steps for miniaturized thin-film filters regarding thickness and cost reduction are presented in this paper. We have developed substrate-free miniaturized coarse

Table 1. Single-Mode, Lens-Free WDM Setups Based on Miniaturized Thin-Film Filters on Few-Micrometer Polymer Substrates[a]

Pass Wavelength	Insertion Loss	Source
1.55 μm	−0.5 dB	[10]
1.31 μm	−1.1 dB	[25]
1.625 μm	−1.78 dB	[26]
1.31 μm, 1.49 μm, and 1.64 μm	−1.25 dB to −1.64 dB	[27]
1.31 μm and 1.55 μm	−1 dB to −1.2 dB	[28]

[a]Examples from the literature.

WDM (CWDM) thin-film filters, based on a sacrificial substrate approach, reducing the thickness of the filter down to the functional layers. Liu *et al*. have reported on freestanding miniaturized optical thin-film filters for an application with light emitting diodes [11]. However, the filters were transferred onto elastomer stamps or polyimide substrates, and the sacrificial layer was produced by sputtering a metal layer (copper, magnesium, or germanium). Ockenfuss and Klinger have published a sacrificial substrate approach based on a water soluble sodium chloride (NaCl) layer for a WDM application [12]. However, they reported that the NaCl layer was first covered with a thick layer of SiO_2 for protection. Since this was the first deposited layer after the NaCl, it remains on their substrate-free WDM filter, adding to the total thickness. Additionally, they re-attached the filters to different substrates due to their special focus on temperature stability and because their filters are not intended for single-element application in fibers.

In this contribution, we report on the production process for substrate-free CWDM filters based on a cost-efficient sacrificial polymer layer, which completely dissolves in water [13], and analyze the filter transmission performance in comparison to filters on thin polymeric substrates as well as the deformation induced by coating stress. The filters are designed for direct insertion between cleaved fiber ends without additional elements. This way, simplex patch-cord-style single-mode fiber wavelength selective devices, according to [14], which transmit one CWDM channel and effectively block the others, can be realized.

2. EXPERIMENTAL

In this work, we focus on a CWDM filter with a pass channel at 1311 nm, necessary for a telecommunication application, as an example of our substrate-free miniaturized filter production process. This process can directly be applied to other thin-film optical coatings produced by IBS.

A. Sacrificial Substrate

Our approach is to deposit the thin-film coating on top of a sacrificial layer that is completely dissolvable. The sacrificial layer consists of polyvinyl alcohol (PVA) with about 99 mol% degree of hydrolysis and is water soluble. It is a non-toxic material. We used a 3 to 5 wt%, double filtered PVA solution in deionized water and achieved a smooth surface with a roughness of about 1 nm, suitable for optical coatings, by spin coating commercially available polished silicon wafers with static dispense and subsequent air drying. A clean processing environment in a laminar flow box is particularly important, as we have found that imperfections such as inclusions or comet streaks in the PVA layer can lead to premature delamination of the actual thin-film filter coating.

B. IBS Thin-Film Filter

The wavelength division effect is generated by a bandpass filter design, which has a high transmittance around 1311 nm (IL better than −0.2 dB for 1304.5 nm to 1317.5 nm) and reflects the other CWDM channels from 1264.5 nm to 1617.5 nm (minimum isolation 30 dB). This design fulfills the standard regarding the IL communicated in IEC 61753-043-02:2022 [14]. To keep the optical path length for the transmitted wavelengths around 1311 nm short, a preferable thin design is beneficial, because the filter is applied without collimating lenses. Subject to these conditions, we used two materials for the filter that achieve a high refractive index contrast in our IBS process: titania with $n_{TiO_2} = 2.30$ and silica with $n_{SiO_2} = 1.46$ at 1311 nm. With these oxide materials, we designed a CWDM filter with 73 layers, which is index matched to a standard step-index single-mode fiber used in telecommunications. It deviates from a typical cavity design to reduce the thickness at the expense of performance. The total design coating thickness was 22.87 μm, and the individual layer thicknesses were below 390 nm. A high layer thickness accuracy was maintained during the IBS coating production by *in situ* high-resolution broadband monitoring [15] based on transmission measurements on a fused silica sample placed in the same substrate holder as the PVA coated silicon wafers and is simultaneously coated. We observed a good adhesion of the first sputtered layer (TiO_2) to the sacrificial PVA layer.

C. Filter Miniaturization and Transfer to Tape

We realize the miniaturization in the areal extent according to the required size in the application, by segmentation of the finished coating with a picosecond laser process into individual elements [16]. The silicon wafer remains as a whole and is cut as little deep as possible by the segmentation process, which reduces the contamination of the filter surfaces by debris. In this study, the filter elements are squares with an edge length of 250 μm, and cutting loss is 4 μm for each groove at the bottom of the laser cut. With our current IBS plant optimized for the production of such miniaturized filters, we can coat up to seven wafers with a diameter of 76.2 mm in parallel, each exhibiting a homogeneous area (not affected by edge shadowing effects of the substrate holder, layer-thickness uniformity within ±0.2%) with approximately Ø 55 mm. Depending on the filter specifications and the tolerance of the design, up to 250,000 such filter elements can be produced in a single coating run on the seven wafers. For the application discussed in this paper, we estimate a yield of about 79,000 filters per coating run due to the requirements regarding the spectral position of the passband. We have demonstrated that different edge lengths of the elements between 25 μm and 1 mm are also possible, depending on the IBS coating thickness [13].

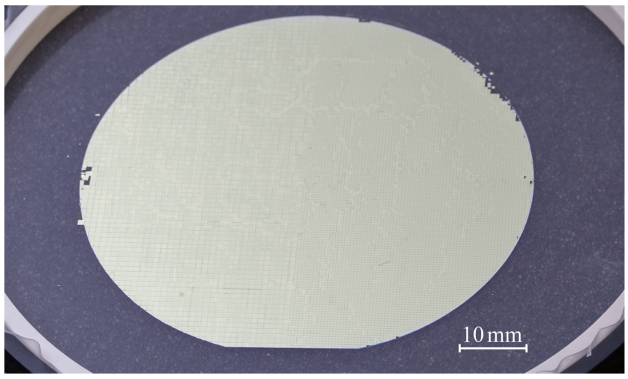

Fig. 1. Substrate-free miniaturized filter elements with an edge length of 1 mm (left hand side) and 0.5 mm (right hand side), transferred from wafer to UV releasable tape, in a grip ring.

The removal of the sacrificial substrate completes the miniaturization by significantly reducing the thickness. Since the soluble PVA is the first layer on the silicon wafer, in this step, the filter elements are detached from the substrate. We applied a releasable tape to the front side of the filter elements before completely dissolving the PVA layer in a magnetic stirrer water bath at about 80°C. As exemplarily shown in Fig. 1, we achieved a transfer rate of over 95% of the elements to the tape, while their relative positions, as on the wafer, were preserved. The adhesion of the tape can be reduced later, depending on the type of tape by either UV illumination or heating, and the substrate-free miniaturized thin-film filters can be picked up individually, without residues remaining.

3. STRESS INDUCED DEFORMATION OF SUBSTRATE-FREE MINIATURIZED FILTERS

Compressive stress is a well known phenomenon in optical coatings deposited by IBS and causes a cap-like deformation of the coated substrate in the case of an isotropic, homogeneous coating. The stress induced deformation is stronger for thinner substrates [17], and when parts of the coatings are completely detached from the substrate, e.g., by delamination, their radius of curvature shrinks compared to how much the coating had bent the substrate before. This can even lead to the formation of rolls [18,19]. Thus, since detaching a multilayer system with intrinsic stress from its stiff substrate can cause stronger deformation, we have investigated how the coating stress affects the substrate-free miniaturized filters.

A. Calculation of the Coating Stress

The stress of an isotropic, homogeneous thin film, σ_{rr}, can be determined from the experimentally accessible radius of curvature R of a substrate, coated by this thin film, according to [20]

$$\sigma_{rr} = -\frac{E_{\text{subs}} d_{\text{subs}}^2}{6(1-\nu_{\text{subs}}) d_{\text{film}}} \frac{1}{R}. \tag{1}$$

In Eq. (1), E_{subs} is Young's modulus of the substrate, ν_{subs} is Poisson's ratio of the substrate, d_{subs} is the thickness of the substrate, and d_{film} is the thickness of the thin film. This formalism is valid only in the case of a circular thick substrate compared to the thin film, i.e., the fused silica sample that is always included in each coating run for layer thickness monitoring. The data sheet of this fused silica (OHARA Sk-1300) contains the required values $E_{\text{subs}} = 71.39$ GPa and $\nu_{\text{subs}} = 0.17$.

B. Measurement and Evaluation of the Deformation

We have applied two different methods for measuring the curvature: interferometry and laser scanning microscopy. The interferometry approach is suitable for the coated fused silica sample, and laser scanning microscopy is applicable for both the fused silica sample and substrate-free miniaturized filter.

1. Interferometry

An interferometer (ZYGO VeriFire XPZ, measurement wavelength $\lambda = 633$ nm) was used to measure the surface flatness of the sample from the reflected wavefront. In a first step, the interferometer setup was focused and the lateral dimensions were calibrated with the help of an uncoated fused silica sample of a known diameter (Ø 25 mm). Due to its strong curvature, for the measurement of the actual Ø 38 mm coated sample, only a small spot in the center of the sample, typically below 4 mm × 4 mm, could be evaluated. Therefore, the measurements were carried out at the maximum zoom level of the instrument.

An average radius of curvature was fitted to the measured data with the interferometer software (ZYGO Mx 6.1.0.5). The measurement procedure including lateral calibration was repeated six times under different rotations of the sample. This resulted in an average measured radius of curvature of $R = 1.426$ m with a standard deviation of 0.008 m. From Eq. (1), it follows that the compressive stress of the coating is $\sigma_{rr} \approx -0.44$ GPa.

2. Laser Scanning Microscopy

We used the stitching method of the laser scanning microscope (Keyence VK-X1100, wavelength $\lambda = 404$ nm) to generate images of the coated fused silica sample and the freestanding miniaturized filter. We processed the images with the software of the manufacturer (MultiFileAnalyzer 2.1.3.89 and VK Analyse-Modul 4.0.0.0).

We measured the coated fused silica sample with a lens magnification of 2.5×. The image was stitched from 10 × 7 individual images. We captured a stitched image of a bare silicon wafer of the same size and subtracted this image as a flat reference. Both images were individually corrected for tilt of the samples beforehand. Profile scans across the fused silica sample in the resulting stitched image were fitted with the software with a circle and yielded radii of curvature from 1.16 m to 2.64 m. From Eq. (1), it follows that the compressive stress of the coating is between −0.24 GPa and −0.54 GPa. Deviations compared to interferometry might be due to the smaller analyzed area of the interferometry, meaning that the actual deformation is not an idealized cap shape.

We measured the miniaturized filter in the laser scanning microscope with an objective lens with a magnification of 50×. This way, two images have to be stitched vertically to display the

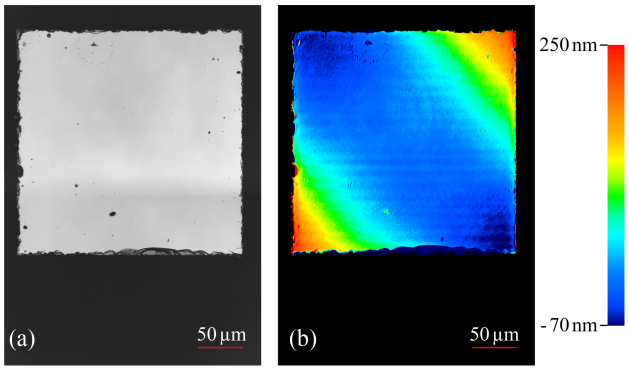

Fig. 2. Laser scanning microscopy of an individual freestanding miniaturized CWDM filter. The filter is shown bottom-up, with the first deposited layer facing the detector. (a) Laser intensity, stitched from two images. A slight vignetting on the upper edge of the lower image can be seen in the lower third of the filter, but it did not affect the height measurement. (b) Resulting height image in false color coding, displaying a saddle-shaped deformation. The horizontal lines and slightly visible $\varnothing \approx 120$ µm ring shaped structure in the upper left quarter of the filter are image artifacts.

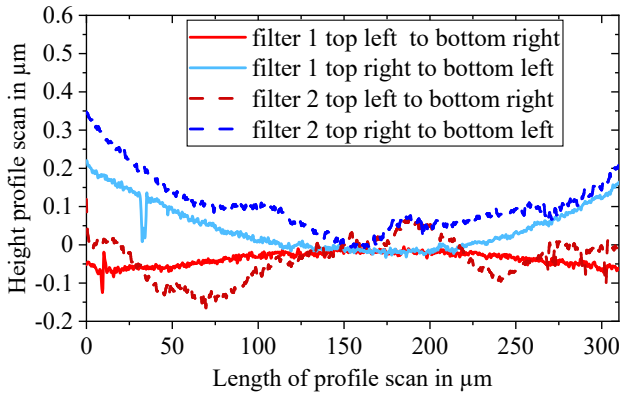

Fig. 3. Profile scans along the diagonal of substrate-free miniaturized CWDM filters. Generated from height images, captured with laser scanning microscopy.

whole 250 µm × 250 µm filter. The laser scanning microscope causes horizontal lines as image artifacts. Since they are not at the same position on every image, averaging over eight such stitched images reduced these artifacts. The stitched plane reference image of an uncoated silicon wafer was also averaged over eight captures and then subtracted from the filter image. Additional image processing consisted of tilt correction, adjusting the height range, and setting the dark cut level of laser intensity to eliminate the noisy region outside the filter surface. The resulting height images of the substrate-free miniaturized filters revealed a saddle-shaped deformation as depicted in Fig. 2.

The finding was confirmed by laser scanning microscopy of a second miniaturized substrate-free filter, although in this case, the surface was less even. Profile scans along the filter diagonals are shown in Fig. 3.

The fitted radii of curvature were smaller for the substrate-free filter than for the coated fused silica sample. For the convex direction, they are 20 cm for filter 1 and 4 cm for filter 2 and for the concave direction, 5.9 cm for filter 1 and 4.1 cm for filter 2.

4. COMPARISON TO MINIATURIZED FILTERS ON POLYMER SUBSTRATE

We have previously reported on our miniaturized thin-film filters on a polymer substrate [15], where the spin coated polymer layer is of optical quality and has a typical thickness of 4 µm. To compare these to the novel type of filters, we considered the case of two standard single-mode fibers with FC/PC connectors with a miniaturized CWDM filter element for 1311 nm with an edge length of 250 µm placed between the facets of the fibers. Figure 4(b) shows a microscopy image of such a filter placed on a fiber end facet covering both the core and cladding of the fiber.

A. Theoretical Comparison Based on Gaussian Beam Approximation

To assess the theoretically expected IL improvement of the substrate-free filter under the assumption of perfect fiber-to-fiber coupling without lateral misalignment, we used several approximations. We assumed that a Gaussian beam, with a beam waist w_0, located at the end facet of the fiber and equal to the half mode field diameter (MFD) of the fiber, is valid for the divergence of the electric field, emitted from the fiber, as well as the accepting fiber. This is a good approximation for the LP_{01} mode of the fiber according to [21]. The MFD is 9.2 µm at a wavelength of 1.31 µm. From the overlap integral of these electric fields, the coupling efficiency follows as [22]

$$T = 1/\sqrt{1 + \left(\frac{\lambda z}{2\pi w_0^2}\right)^2}, \tag{2}$$

where z is the propagation distance, and $\lambda = \lambda_{\text{vacuum}}/n$ is the wavelength in the medium between fibers. For the refractive index n, we used a weighted average of the two materials in the thin-film filter ($n_{\text{substrate-free}} = 1.81$ at 1.311 µm). For the case of the filter on the polymer layer, the refractive index of the 4 µm polymer is also considered, resulting in a slightly lower weighted average refractive index ($n_{\text{with polymer substrate}} = 1.75$ at 1.311 µm). To take into account internal reflections of the transmitted beam inside the thin-film filter, we calculated the beams' propagation distance z via the group delay at 1.311 µm. The group delay GD is calculated by thin-film software for the design when it is integrated inside a medium with a refractive index similar to the effective refractive index of the fiber. The GD is longer in the transmitted channel compared to the reflected wavelengths, with local maxima near the edges of the

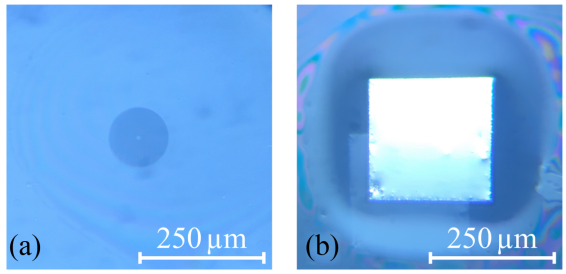

Fig. 4. Images taken through a fiber microscope. (a) Fiber end facet with index matching gel. The 125 µm cladding and 8.2 µm core are visible. (b) Substrate-free, miniaturized filter placed within the drop of index matching gel.

passband. In the center of the transmitted channel at 1311 nm, it evaluates to $GD_{\text{substrate-free}} = 448.548$ fs for the substrate-free case and $GD_{\text{with polymer substrate}} = 448.477$ fs for the filter on 4 μm polymer. This group delay has to be multiplied by the group velocity v_g to give the propagation distance

$$z = GD \cdot v_g = GD \cdot c/n_{\text{group}} = GD \cdot c/\left(n(\lambda) - \lambda \frac{\partial n(\lambda)}{\partial \lambda}\right). \quad (3)$$

The group index n_{group} includes the derivative of the refractive index with respect to the wavelength. Since we describe the refractive indices of all materials with Sellmeier equations, we took the derivative of a weighted average of these functions and evaluated it at 1.311 μm. The resulting propagation distances are $z_{\text{substrate-free}} = 72.61$ μm for the substrate-free case and $z_{\text{with polymer substrate}} = 75.11$ μm for the filter on the thin polymer layer. Note that these propagation distances are about three times larger than the geometrical thickness of the thin-film filter. Inserting Eq. (3) into Eq. (2) and considering that the maximum transmission of the design of the thin-film filter for a plane wave at 1.311 nm is 99.5%, we obtain a theoretical maximum of the transmission in the measurement setup of 91.67% (−0.38 dB) for the miniaturized filter on a 4 μm polymer substrate and 92.53% (−0.34 dB) for the substrate-free filter, which equals an improvement of 0.86% or 0.04 dB.

B. Measurement of Spectral Performance

We measured the IL and return loss (RL) of the described setup with an EXFO All-Band Component Analyzer system IQS-12008. The system allows to measure IL and RL within one measurement in the wavelength range from 1250 nm to 1635 nm. In a first step, the system is calibrated by directly connecting the input and output optical connectors. For the filter performance measurement, we centered the filter element between these connectors, with an index matching gel applied to the connector surfaces. For each sample wafer, we measured 15 filter elements that were picked along the diagonal of the wafer, respectively, the tape, perpendicular to the wafer flat, as illustrated in Fig. 5. The distance between the picked filters was

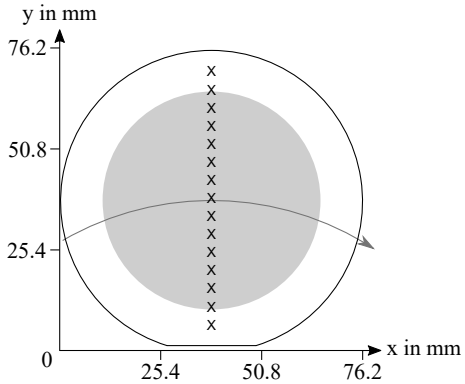

Fig. 5. Location of the measured filter elements on a Ø 76.2 mm sample wafer diagonal, marked by black X's. The light gray shaded area corresponds to the Ø 55 mm homogeneous coating area (uniformity ±0.2%), which is not affected by shadowing effects from the edges of the substrate holder. The arrow indicates the direction of the rotation of the substrate holder during the coating process.

20 rows of elements, which equals 5.08 mm. This way, the measured data reflect the layer thickness gradient along the wafer. We measured the filters directly after picking them, without further treatment.

C. Results

Figure 6 shows the spectral performance of exemplary CWDM filter elements, with and without a substrate, from the same coating run. Here, the substrate-free filter with the best measured IL at 1311 nm of −0.7 dB, which equals 85.11% transmission (filter originating from the sixth position from the top in Fig. 5), is plotted together with the filter on a polymer substrate that was closest in layer thickness and therefore matched best in the measured spectral shape, for comparability. This filter on a thin polymer substrate reached an IL of −0.94 dB at 1311 nm, which equals 80.54% transmission. One filter on a thin polymer substrate reached a lower IL of −0.92 dB (80.91% transmission), but its pass channel was shifted to higher wavelengths due to a slightly higher coating rate at its position on the wafer diagonal. The isolation to the adjacent channels (1271 nm and 1331 nm) was below 40 dB. The isolation to the other channels was below 60 dB.

On average, the 12 substrate-free filters from the approximately 55 mm long homogeneous part of the diagonal reached a maximum transmission of 82.83% (standard deviation of this value from the different measured filters: 1.77%). Filters originating from the same relative positions with a polymer substrate reached 78.58% maximum transmission on average (standard deviation: 2.65%). This equates to about 4.25% higher transmission in the pass channel for the substrate-free filters on average. See Data File 1 and Data File 2 for underlying values of these results.

5. DISCUSSION

The results of the curvature measurements revealed that the substrate-free filters are more strongly curved than the fused silica sample, which is coated with the same multilayer filter. With radii in the centimeter range, the curvatures of free-standing filters are still significantly less than the curvatures of lenses, which are used for beam shaping of radiation emitted from single-mode fibers (millimeter-range radii). Therefore, we expect a negligible beam shaping effect due to the filter element curvature in our fiber setup. Within ∼ 53 μm^2 of the fiber core, the miniaturized, substrate-free filters are approximately flat. It has to be noted that the substrate-free filter lay on the bottom of a polypropylene wafer container during microscopy, and besides stress, other forces between non-conductive materials might have played a role in the deformation of the filters. However, such forces may as well play a role in the final application of the filter, inserted with index matched glue between fibers.

Regarding the transmission performance of the filters, our simplified theoretical model clearly underestimates the losses occurring in the measurement setup. Additionally, while a slight improvement for the substrate-free case compared to the same layer stack on a thin polymer substrate is predicted, the measurement revealed a much higher gain in transmittance. However, a full spectral solution to Maxwell's equations for the LP_{01} mode

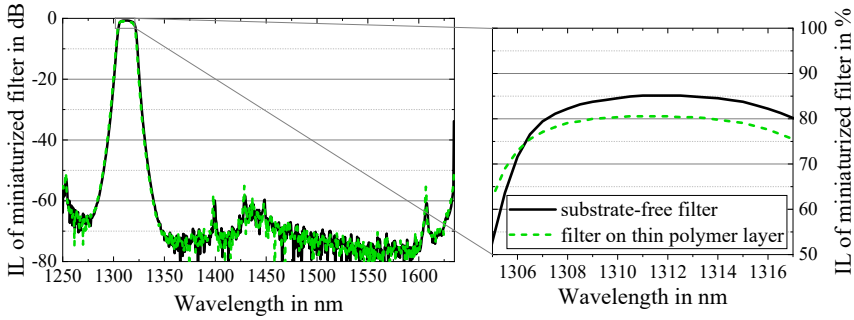

Fig. 6. Comparison of the transmission through miniaturized CWDM filters from the same coating run, measured between single-mode fibers, shown in dB for the telecom wavelength range on the left hand side and shown in detail for the passband in percent. The green dashed curve corresponds to a filter on a 4 μm polymer layer. It has an IL of −0.94 dB at 1311 nm. The solid black curve corresponds to the best measured substrate-free filter, where the IL at 1311 nm is −0.7 dB, which equates to an improvement in transmission of 4.6%.

in the 3D geometry of the filter between fibers, which would give an accurate prediction, is beyond the scope of this work. Additional loss channels could also play a role including coating rate errors, irregular layer thickness errors, and scattering. We measured the total scattering of the wafers at 532 nm. The wafers coated with the 4 μm polymer layer exhibited a slightly increased scattering (5×10^{-4}) compared to the wafers coated with PVA (9×10^{-5}).

For the final device, temperature stability can additionally influence the transmission performance via the spectral position of the passband. The environmental tests specified in IEC 61753-043-02:2022 allow a change in transmission of no more than 0.4 dB during a tested temperature range from −10°C to +60°C at the tested wavelength [14]. While we have not measured the temperature coefficient of our substrate-free filters, we estimated the effect based on temperature coefficients of the refractive index and linear expansion of amorphous thin-film materials quoted from Essential Macleod (Thin Film Center Inc) software. The calculation for the coefficients in this software is based on a publication by Takashashi [23]. For silica, the value given in the software for the temperature coefficient of refractive index is 9×10^{-6}/°C, and for the thermal expansion coefficient, it is 5.5×10^{-7}/°C. For titania, the temperature coefficient of refractive index is 2.6×10^{-5}/°C, and the thermal expansion coefficient is 1.1×10^{-6}/°C. With

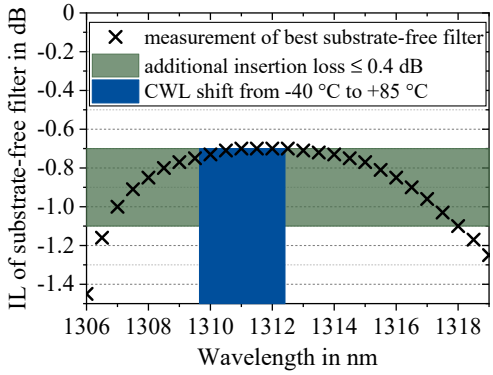

Fig. 7. Measurement of the IL of the substrate-free filter in dB (black crosses) and allowed range for additional ILs of ≤ 0.4 dB during standardized temperature test from −10°C to +60°C (green shaded area) in comparison to the estimated CWL shift of the filter for an even wider temperature range of −40°C to +85°C (blue area).

these values, we calculated our thin-film design with changed physical and optical thickness of each layer and modified refractive indices for a temperature shift of −32°C and +38°C from room temperature (22°C). The calculation resulted in a central wavelength (CWL) shift of −0.76 nm and +0.86 nm. When performing the calculation for a wider temperature range of −40°C to +85°C, the CWL shifts in the range of −1.35 nm to +1.41 nm. Figure 7 depicts this range of CWL shift and the range of allowed additional ILs during temperature tests, starting from the measured IL of −0.7 dB at 1311 nm. According to this estimation, the CWL shift induced additional IL stays well within the specifications.

6. SUMMARY AND CONCLUSION

We have created novel miniaturized, substrate-free CWDM filters, which have an improved transmission performance compared to previously reported miniaturized filters on a thin polymer layer. Our measurements showed an improvement in transmission in the pass channel of 4.25% on average for filters from the same coating run. With an IL of −0.7 dB at 1311 nm and an isolation of more than 40 dB to the adjacent CWDM channels and more than 60 dB to all other CWDM channels, the substrate-free filters come close to the performance of reported WDM components based on direct coating of fiber end facets. However, the miniaturized filter production process allows for a higher yield. Notably, the novel filters are more cost efficient than previously reported miniaturized filters, because the expensive polymer layer of optical quality is replaced by the cheaper water-removable PVA layer. PVA is also cheaper than previously reported sacrificial metal layers. In comparison to water soluble sacrificial layers made of NaCl, it is more environmentally stable and does not need a protective capping layer. The substrate-free filters are very versatile regarding the application because the multi-layer design can be matched directly to the surrounding medium, and no substrate refractive index has to be considered. The measured radii of curvature of the miniaturized, substrate-free filters are in the centimeter range. This means that they are approximately flat when used between single-mode fibers or within photonic integrated circuits. Our estimations show that the temperature stability of the filter is

sufficient to fulfill the standardized environmental test requirements of simplex patch-cord-style single-mode fiber wavelength selective devices according to IEC 61753-043-02:2022 [14]. Additionally, the handling of the filter elements, for example, in an automated assembly process, is simplified by the transfer to a releasable tape. These advantages make the novel substrate-free filters a highly relevant component for hybrid integrated photonics applications.

Funding. Deutsche Forschungsgemeinschaft (390833453, EXC 2122); Bundesministerium für Wirtschaft und Energie (KK5111701KG0, KK5114401KG0).

Acknowledgment. Portions of this work were presented at the Optical Interference Coatings Conference in 2022, paper MD.5 [24]. The authors thank the Deutsche Forschungsgemeinschaft (DFG, German Research Foundation) for funding this work under Germany's Excellence Strategy within the Cluster of Excellence PhoenixD. The project "Wellenlängenselektive CWDM Patchkabel auf Basis von integrierten Dünnschichtfiltern" was funded by the German Federal Ministry for Economic Affairs and Energy.

Disclosures. The authors declare no conflicts of interest.

Data availability. Data underlying the results presented in this paper are available in Data File 1 and Data File 2.

REFERENCES

1. R. Blum, "Integrated silicon photonics for high-volume data center applications," Proc. SPIE **11286**, 112860M (2020).
2. H. Ehlers and D. Ristau, "Chapter 4 - production strategies for high-precision optical coatings," in *Optical Thin Films and Coatings*, A. Piegari and F. Flory, eds., 2nd ed., Woodhead Publishing Series in Electronic and Optical Materials, (Woodhead Publishing, 2018), pp. 103–140.
3. R. Watanabe, Y. Fujii, K. Nosu, and J. Minowa, "Optical multi/demultiplexers for single-mode fiber transmission," IEEE J. Quantum Electron. **17**, 974–981 (1981).
4. P. Lissberger, A. Roy, and D. McCartney, "Narrowband position-tuned multilayer interference filter for use in single-mode-fibre systems," Electron. Lett. **21**, 798–799 (1985).
5. D. McCartney, P. Lissberger, and A. Roy, "Recent developments in the production of narrowband position tuned interference filters for wavelength multiplexed optical fibre systems," Opt. Commun. **64**, 338–342 (1987).
6. H. Yanagawa, H. Hayakawa, T. Ochiai, K. Watanabe, and H. Miyazawa, "Low-loss single-mode wavelength multiplexer," in *Optical Fiber Communication* (Optica Publishing Group, 1988), paper ThJ1.
7. A. Reichelt, H. Michel, and W. Rauscher, "Wavelength-division multi demultiplexers for two-channel single-mode transmission systems," J. Lightwave Technol. **2**, 675–681 (1984).
8. H. Yanagawa, T. Ochiai, H. Hayakawa, and H. Miyazawa, "Fused taper/filter hybrid single-mode wavelength division multi/demultiplexer," Electron. Lett. **24**, 312–313 (1988).
9. H. Yanagawa, T. Ochiai, H. Hayakawa, and H. Miyazawa, "Fused taper/filter hybrid three-channel single-mode wavelength division multi/demultiplexer," in *Optical Fiber Communication Conference* (Optica Publishing Group, 1989), paper WQ7.
10. T. Oguchi, I. Noda, H. Hanafusa, and S. Nishi, "Dielectric multilayered interference filters deposited on polyimide films," Electron. Lett. **27**, 706–707 (1991).
11. C. Liu, Q. Zhang, D. Wang, G. Zhao, X. Cai, L. Li, H. Ding, K. Zhang, H. Wang, D. Kong, L. Yin, L. Liu, G. Zou, L. Zhao, and X. Sheng, "High performance, biocompatible dielectric thin-film optical filters integrated with flexible substrates and microscale optoelectronic devices," Adv. Opt. Mater. **6**, 1800146 (2018).
12. G. J. Ockenfuss and R. E. Klinger, "Ultra-low-stress thin-film interference filters," Appl. Opt. **45**, 1364–1367 (2006).
13. A. K. Rüsseler, F. Carstens, L. Jensen, S. Bengsch, and D. Ristau, "Applying sacrificial substrate technology to miniaturized precision optical thin-film coatings," Proc. SPIE **11872**, 118720G (2021).
14. "Fibre optic interconnecting devices and passive components - performance standard - part 043-02: Simplex patch-cord style single-mode fibre wavelength selective devices with cylindrical ferrule connectors for category c - controlled environment," IEC 61753-043-02:2022 (2022).
15. F. Carstens, H. Ehlers, S. Schlichting, L. Jensen, and D. Ristau, "High-resolution optical broadband monitoring for the production of miniaturized thin-film filters," in *Optical Interference Coatings Conference (OIC)* (Optica Publishing Group, 2019), paper WA.7.
16. R. Kling, T. Eschenberg, F. Siegel, U. Klug, and A. Ostendorf, "Picosecond lasers in industrial applications," in *Pacific International Conference on Applications of Lasers and Optics* (Laser Institute of America, 2008), pp. 739–744.
17. S. L. Prins, A. C. Barron, W. C. Herrmann, and J. R. McNeil, "Effect of stress on performance of dense wavelength division multiplexing filters: optical properties," Appl. Opt. **43**, 626–632 (2004).
18. G. G. Stoney, "The tension of metallic films deposited by electrolysis," Proc. R. Soc. London A **82**, 172–175 (1909).
19. O. G. Schmidt and K. Eberl, "Thin solid films roll up into nanotubes," Nature **410**, 168 (2001).
20. H. Bach and D. Krause, eds., *Thin Films on Glass* (Springer, 2003), p. 116.
21. A. M. Kowalevicz, Jr. and F. Bucholtz, "Beam divergence from an SMF-28 optical fiber," Tech. rep. (Naval Research Laboratory, 2006).
22. W. Karthe and R. Müller, *Integrierte Optik* (Akadem. Verlagsgesellschaft Geest & Portig, 1991), Chap. 4.
23. H. Takashashi, "Temperature stability of thin-film narrow-bandpass filters produced by ion-assisted deposition," Appl. Opt. **34**, 667–675 (1995).
24. A. K. Rüsseler, P. Gehrke, G. A. Hoffmann, G. Schönsee, A. Thiel, M. Vitt, A. Wienke, and D. Ristau, "Substrate-free miniaturized coarse wavelength division multiplexing filters," in *Optical Interference Coatings Conference (OIC)* (Optica Publishing Group, 2022), paper MD.5.
25. Y. Inoue, T. Oguchi, Y. Hibino, S. Suzuki, M. Yanagisawa, K. Moriwaki, and Y. Yamada, "Filter-embedded wavelength-division multiplexer for hybrid-integrated transceiver based on silica-based PLC," Electron. Lett. **32**, 847–848 (1996).
26. N. Araki, H. Izumita, N. Honda, and M. Nakamura, "Extended optical fiber line testing system using new eight-channel l/u-band crossed optical waveguide coupler for l-band WDM transmission," J. Lightwave Technol. **21**, 3316–3322 (2003).
27. J. H. Song, K. S. Lee, and Y. Oh, "Triple wavelength demultiplexers for low-cost optical triplexer transceivers," J. Lightwave Technol. **25**, 350–358 (2007).
28. N. Keil, Z. Zhang, C. Zawadzki, C. Wagner, A. Scheibe, H. Ehlers, D. Ristau, J. Wang, W. Brinker, and N. Grote, "Ultra low-loss 1 × 2 multiplexer using thin-film filters on polymer integration platform," Electron. Lett. **45**, 1167–1168 (2009).